Railway track degradation: The contribution of a spatially variant support stiffness - Local variation

Sadri, Mehran; Lu, Tao; Steenbergen, Michael

DOI
10.1016/j.jsv.2019.05.006

Publication date
2019

Document Version
Accepted author manuscript

Published in
Journal of Sound and Vibration

Citation (APA)
Sadri, M., Lu, T., & Steenbergen, M. (2019). Railway track degradation: The contribution of a spatially variant support stiffness - Local variation. *Journal of Sound and Vibration*, *455*, 203-220. https://doi.org/10.1016/j.jsv.2019.05.006

Railway Track Degradation: the Contribution of a Spatially Variant Support Stiffness - Local Variation.

Mehran Sadri, Tao Lu and Michaël Steenbergen*

Delft University of Technology, Faculty of Civil Engineering and Geosciences, Railway Engineering Group, Stevinweg 1, 2628 CN Delft, The Netherlands

* Corresponding author,
Tel: +31 15 2783385; Email address: m.j.m.m.steenbergen@tudelft.nl

Abstract

This study addresses the contribution of spatial variance in the railway track support stiffness to the expected long-term track degradation. Hereto, a novel frequency-domain model is developed with a double periodicity 'layer', capable of dealing with both sleeper periodicity and arbitrary non-uniformity in track properties. The model application focuses on a locally reduced support stiffness (hanging sleeper) along the track. The resulting susceptibility to degradation is assessed by quantifying the mechanical energy dissipated over the influence length under a moving train axle. Different descriptions of this energy amount are benchmarked with respect to their predictive value. In the presence of a degraded sleeper support, hanging sleepers are found to develop faster with increasing train speed; the speed effect may be estimated as roughly linear. Moreover, degradation increases progressively with an increasing local relative stiffness reduction. Coincidence of the train speed corresponding to the sleeper passing frequency with the first resonance peak of the system leads to severely increased degradation; increased damping however attenuates dissipation peaks at resonant speeds and shifts their position upwards. The effect of a degraded support is most significant on soft subgrades. The effect of multiple degraded sleeper supports increases up to three sleepers, for any train speed. With respect to the system parameters, particularly the railpad stiffness has significant effect; especially for high-speed tracks a high pad stiffness is very unfavorable. Other effective control parameters in the case of degraded sleeper supports are the sleeper spacing and the rail cross-sectional properties; for example replacing a 54E1 with a 60E1 rail profile may reduce degradation with roughly 30% on high-speed track. An increasing unsprung vehicle mass is unfavorable for track degradation, again with the effect increasing with the train speed. The developed methodology is shown to have significant potential with respect to railway track design in terms of multi-parametric optimization for concrete cases with a given input in terms of soil properties and operational regime.

Keywords: Track degradation, Spatial variance, Hanging sleeper, Energy dissipation, Track stiffness, Track settlement.

1. Introduction

The physical understanding and prediction of the degradation of classical ballasted railway track, in terms of the development of uneven track settlement over the loading history, remains a challenge for fundamental-theoretical research. In a previous study by the authors [1], three distinct major and primary mechanisms within the train-track system were identified as responsible for long-term track degradation: wheel out-of-roundness (OOR) of the rolling stock, longitudinal variability of the cross-sectional properties and track irregularity. From these mechanisms, the second and third are directly associated with the track condition. The previous study dealt with perfectly uniform track and took into account only the second mechanism in as far as it is inherent to classical ballasted railway track, i.e. the periodicity of the support stiffness induced by the discrete sleeper spacing. Because of its inherence to classical track, it is not commonly perceived by railway engineers as 'spatial variance' of track properties. The present study aims to extend the previous one by including also non-periodical (and arbitrary) spatial variance. The most relevant form of spatial variance in practice is the one that occurs in the support stiffness and typically manifests itself in two principal ways:

i. Local settlement of the ballast under a sleeper (or eventually multiple sleepers in series), eventually leading to contact loss in unloaded condition; also known as degraded sleeper support or, eventually, 'hanging sleepers'. This is the main form to be considered in the applied part of the present study.

ii. More global variation in support stiffness over the sleepers due to spread in ballast/soil properties, composition and geometry of the granular matrix, and the degree of compaction. The study of this form is reserved for future work.

Whereas the latter type is not generally considered as 'degradation', it is present in each railway track (in the form of a 'stiffness profile', see e.g. [2]), even at the initial stage. The first one on the contrary is considered as 'damage', and even a damage type that can grow and expand progressively (an example is shown in Fig. 1). Both of them are of paramount importance in the study of railway track degradation.

Fig. 1. Hanging sleepers and track degradation (mud pumping)

The subject in general and both specific forms *i* and *ii* have received attention in the scientific literature, which can be summarised under three categories with different perspectives. The first perspective is the establishment of an empirical non-linear constitutive model or settlement law for the ballast/subgrade under cyclic loading, mainly from laboratory or small-scale field testing. Such a material model can then serve as an input in computational train-track interaction models that predict track settlement. This approach was taken in relatively early research [3-6]. A second perspective considers the track stiffness as a measure for the track quality and durability in terms of geometry, and therefore investigates possibilities for defining and continuously measuring this track stiffness and eventual variability in various ways; see e.g. [7-10]. A third perspective departs from support stiffness variation as a matter of fact and studies its role on dynamic train-track interaction, described typically at the level of the wheel-rail interface in terms of dynamic contact forces or rail displacements. In the framework of this investigation, especially those studies are relevant that consider local variation due to reduced sleeper support or hanging sleepers; these include [11-17]. These studies use analytical-numerical models in the time-domain, a finite element approach and/or multi-body simulation to study the effect on dynamic amplification of contact forces and their effects on the track or vehicle.

The present study does not focus on dynamic train-track interaction force levels, but on a qualitative understanding of the contribution of local non-uniformity of the support stiffness to further structural degradation and a quantification of their relative role in this process. The assessment of the susceptibility to structural degradation is, in analogy to the previous study [1], carried out by quantifying the mechanical energy dissipated in the substructure under moving axle loading. Moreover, the investigation will be done with a frequency-domain model. This choice is unusual due to the mathematical complexity of a frequency-domain analysis in the presence of arbitrary non-uniformity. However, as argued in [1], frequency-domain models are more efficient than time-domain models and even when they cannot deal with non-linearity, they are very suitable for parametric analysis aiming at fundamental understanding,

which is also the aim of this study. The energy loss in the substructure will be described by the viscous damping model. This choice is not experimentally verified and there is no reason that it would represent a most appropriate physical description. On the other hand, it allows a frequency-domain approach and at the same time it is sufficient for the aim of the present work, which is to establish the relative effect of parametric system variation on time-dependent degradation.

In the literature, different analytical/frequency-domain models have been presented that are capable of dealing with some kind of discontinuity, with applications also in railway engineering; they are briefly reviewed. Metrikine et al. [18] analyzed the energy flux in an infinite string resting on an elastic foundation with two types of inhomogeneity (abrupt and smooth changes). The dynamic response of a single-layer track model with a probabilistic distribution of the support stiffness to a moving oscillator was investigated by Andersen and Nielsen [19]. Verichev and Metrikine [20] studied the instability of a rigid mass uniformly moving along an Euler beam resting on a periodically inhomogeneous foundation. Dimitrovova and Varandas [21] studied the influence of an abrupt change in the foundation stiffness on critical velocity of a load moving on a beam of finite length, in order to provide a preliminary insight into the excessive ground vibrations from high-speed tracks with a varying foundation stiffness. The importance of including the vehicle/track interaction in the mathematical model developed in their study was discussed. A similar research project was conducted by Dimitrovova [22] for investigating the transverse vibrations of finite and infinite beams on a piece-wise homogeneous viscoelastic foundation. Baeza and Ouyang [23] employed a model based on modal substructuring and a cyclic boundary condition in order to investigate the effect of a hanging sleeper on the wheel/rail contact force. The dynamic response of a high-speed track with an abrupt change in its foundation stiffness was analyzed in [24] using an extended version of the moving element method (MEM). In the present study, a new approach is proposed, allowing spatial variation of the subgrade properties to be modeled theoretically in the frequency domain. The earlier used frequency-domain model [1], capable of dealing with periodicity due to the discrete sleeper spacing, is extended by introducing a second type of large-scale periodical variation in the support properties, while remaining computationally efficient. The similar approach to [1] allows for cross-benchmarking and a systematical comparison of the results of both studies.

The setup of this paper is as follows. Section 2 presents the theoretical framework of the study by introducing the new model and providing its mathematical formulation. In Section 3, this model is applied to case *i* - the local non-uniformity of the support stiffness, as discussed in the introduction. Section 4 ends with the main conclusions from the work in terms of both theoretical and practical results.

2. Theoretical framework

This section describes the theoretical framework to study spatially variant track, where the latter definition is general, and therefore basically suitable to describe variation of any track property. In order to satisfy the periodicity assumption, a periodic wheel/track model is proposed, incorporating a double 'periodicity layer': small-scale periodicity, accounting for the discrete sleeper spacing, and large-scale periodicity of adjustable length, accounting for major variations in system properties. A schematic overview of the mathematical model is shown in Fig. 2. The frequency-domain two-layer track model consisting of different elements (rail, railpads, sleepers and ballast/subgrade) is coupled to an unsprung wheel mass, uniformly moving along the track, through a linearized contact stiffness, k_H. The track is divided into a number of identical sections, and therefore the model is periodic. Each section consists of N_1+N_3 identical supports and N_2 middle supports with different characteristics. Note that N_1 and N_3 can be chosen as being identical, however this is not necessary. The rail is modeled utilizing the Timoshenko beam theory. As shown in Fig. 2, each support in the track model is composed of a railpad, modeled as a Kelvin-Voigt element, a rigid sleeper mass, and the ballast/subgrade is modelled again as a Kelvin-Voigt foundation [1]. Although the model used in this study for representing the individual sleeper support (i.e. the Kelvin-Voigt element) is not necessarily the most accurate to describe support damping, it is sufficient for the aim of this study, allowing both for an approach in the frequency domain and for a relative comparison of the effects of parametric model variations.

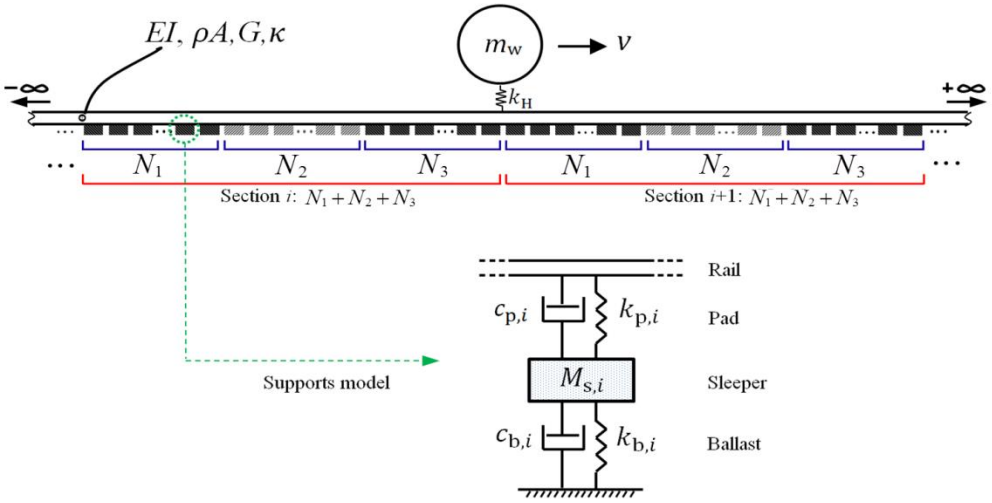

Fig. 2. Schematic overview of the wheel/track model including non-uniformity

The equation of motion for the moving wheel can be written as:

$$m_w \ddot{w}_w(t) = F_c(t) + m_{tot} g, \tag{1}$$

where m_w is the unsprung wheel mass, $m_{tot}g$ half the axle load and $F_c(t)$ is the wheel/rail contact force defined below:

$$F_c(t) = k_H\left(w_b(vt,t) - w_w(t)\right). \tag{2}$$

In the latter equation, $w_b(vt,t)$ and $w_w(t)$ denote the displacement of the rail at the wheel/rail contact point and the wheel displacement, respectively. The equations of motion for the rail can be written by using the Timoshenko beam theory:

$$\rho A\frac{\partial^2 w_b(x,t)}{\partial t^2} - \kappa AG\frac{\partial^2 w_b(x,t)}{\partial x^2} + \kappa AG\frac{\partial \psi_b(x,t)}{\partial x} = -F_c(t)\delta(x-vt) - \sum_{i=-\infty}^{+\infty} R_i(t)\delta(x-il_s), \tag{3}$$

$$\rho I\frac{\partial^2 \psi_b(x,t)}{\partial t^2} - EI\frac{\partial^2 \psi_b(x,t)}{\partial x^2} - \kappa AG\frac{\partial w_b(x,t)}{\partial x} + \kappa AG\psi_b(x,t) = 0, \tag{4}$$

in which ρA, EI, G, κ are the mass per unit length, bending stiffness, shear modulus and the Timoshenko shear coefficient of the rail, respectively. l_s is the sleeper distance, v the speed of the moving unsprung mass, and $\delta(.)$ represents the Dirac-delta function. Moreover, $\psi_b(x,t)$ denotes the angle of rotation for the Timoshenko beam and $R_i(t)$ the interaction force between the rail and the ith support, which is given as:

$$R_i(t) = c_{p,i}\{\dot{w}_b(il_s,t) - \dot{w}_{s,i}(t)\} + k_{p,i}\{w_b(il_s,t) - w_{s,i}(t)\}, \tag{5}$$

where $w_{s,i}(t)$ is the displacement of the ith sleeper. The equation of motion for the ith sleeper can be written as follow:

$$M_{s,i}\ddot{w}_{s,i}(t) = R_i(t) - c_{b,i}\dot{w}_{s,i}(t) - k_{b,i}w_{s,i}(t). \tag{6}$$

The proposed model is periodic with periodic length, $l^* = \left(N_1 + N_2 + N_3\right)l_s$ (i.e. period l^*/v). Therefore, the rail and wheel displacements and the contact force satisfy the following relationships:

$$\begin{cases} w_b(x + l^*, t + \dfrac{l^*}{v}) = w_b(x,t) \\ w_w(t + \dfrac{l^*}{v}) = w_w(t) \\ F_c(t + \dfrac{l^*}{v}) = F_c(t) \end{cases}. \tag{7}$$

Since the rail and wheel responses and the contact force are periodic, Fourier series can be employed to describe them mathematically. The contact force is represented as:

$$F_c(t) = \sum_{m=-\infty}^{+\infty} \bar{F}_m\, e^{jm(\frac{2\pi v}{l^*})t}, \tag{8}$$

in which $\mathrm{j}^2 = -1$ and $\bar{F}_m \left(m \in \mathbb{Z} \right)$ are the unknown amplitudes of the wheel/rail interaction force. The following relationship can be found for the rail displacement (and similarly for the angle of rotation) in the frequency domain:

$$\hat{w}_{\mathrm{b}}(x + l^*, \omega) = \mathrm{e}^{-\mathrm{j}\omega l^* / v} \hat{w}_{\mathrm{b}}(x, \omega), \tag{9}$$

where $\hat{w}_{\mathrm{b}}(x, \omega)$ is the Fourier transform of the rail displacement given as:

$$\hat{w}_{\mathrm{b}}(x, \omega) = \int_{-\infty}^{+\infty} w_{\mathrm{b}}(x, t) e^{-\mathrm{j}\omega t} dt. \tag{10}$$

Taking into account the periodicity of the rail response in Eq. (9), and similarly the periodicity of the angle of rotation, the following relationships can be introduced:

$$\hat{w}_{\mathrm{b}}(x, \omega) = \mathrm{e}^{-\mathrm{j}\omega x / v} \sum_{m=-\infty}^{+\infty} \bar{W}_m(\omega) \mathrm{e}^{\mathrm{j}m\left(\frac{2\pi}{l^*}\right)x}, \tag{11}$$

$$\hat{\psi}_{\mathrm{b}}(x, \omega) = \mathrm{e}^{-\mathrm{j}\omega x / v} \sum_{m=-\infty}^{+\infty} \bar{\psi}_m(\omega) \mathrm{e}^{\mathrm{j}m\left(\frac{2\pi}{l^*}\right)x}, \tag{12}$$

where $\bar{W}_m(\omega)$ and $\bar{\psi}_m(\omega)$ are the frequency-dependent unknown amplitudes of the rail displacement and angle of rotation, respectively. The equations of motion of the rail can be obtained in the frequency domain by taking the Fourier transform of Eqs. (3) and (4):

$$\begin{aligned} -\rho A \omega^2 \hat{w}_{\mathrm{b}}(x, \omega) - \kappa AG \frac{\partial^2 \hat{w}_{\mathrm{b}}(x, \omega)}{\partial x^2} + \kappa AG \frac{\partial \hat{\psi}_{\mathrm{b}}(x, \omega)}{\partial x} = & -\int_{-\infty}^{+\infty} \sum_{m=-\infty}^{+\infty} \bar{F}_m \mathrm{e}^{\mathrm{j}m\left(\frac{2\pi v}{l^*}\right)t} \delta(x - vt) e^{-\mathrm{j}\omega t} dt \\ & - \int_{-\infty}^{+\infty} \sum_{i=-\infty}^{+\infty} R_i(t) \delta(x - i l_{\mathrm{s}}) e^{-\mathrm{j}\omega t} dt, \end{aligned} \tag{13}$$

$$-\rho I \omega^2 \hat{\psi}_{\mathrm{b}}(x, \omega) - EI \frac{\partial^2 \hat{\psi}_{\mathrm{b}}(x, \omega)}{\partial x^2} - \kappa AG \frac{\partial \hat{w}_{\mathrm{b}}(x, \omega)}{\partial x} + \kappa AG \hat{\psi}_{\mathrm{b}}(x, \omega) = 0. \tag{14}$$

The Fourier representations of the responses provided in Eqs. (11) and (12) can now be substituted into the latter equation and the following equation can be derived:

$$\sum_{m=-\infty}^{+\infty} \left\{ \left[\bar{\psi}_m(\omega) \left(\kappa AG + EI \left[\frac{2\pi m}{l^*} - \frac{\omega}{v} \right]^2 - \rho I \omega^2 \right) - \bar{W}_m(\omega) \left(\kappa AG . \mathrm{j} \left(\frac{2\pi m}{l^*} - \frac{\omega}{v} \right) \right) \right] \mathrm{e}^{\mathrm{j}\left(\frac{2\pi m}{l^*} - \frac{\omega}{v}\right)x} \right\} = 0. \tag{15}$$

From the latter equation, the following relationship between the unknown amplitudes of the rail displacement and angle of rotation can be established:

$$\bar{\psi}_m(\omega)=\left(\frac{\kappa AG.\mathrm{j}\left[\frac{2\pi m}{l^*}-\frac{\omega}{v}\right]}{\kappa AG+EI\left[\frac{2\pi m}{l^*}-\frac{\omega}{v}\right]^2-\rho I\omega^2}\right)\bar{W}_m(\omega). \tag{16}$$

This relationship can now be utilized along with Eqs.(11-13), in order to find the following equation:

$$\sum_{m=-\infty}^{+\infty}\left\{\bar{W}_m(\omega)\Lambda_m^*(\omega)\mathrm{e}^{\mathrm{j}(\frac{2\pi m}{l^*}-\frac{\omega}{v})x}+\frac{\bar{F}_m}{v}\mathrm{e}^{\mathrm{j}(\frac{2\pi m}{l^*}-\frac{\omega}{v})x}\right\}=-\sum_{i=-\infty}^{+\infty}\hat{R}_i(\omega)\delta(x-il_{\mathrm{s}}), \tag{17}$$

in which $\Lambda_m^*(\omega)$ is defined as:

$$\Lambda_m^*(\omega)=\kappa AG\left[\frac{2\pi m}{l^*}-\frac{\omega}{v}\right]^2+\kappa AG.\mathrm{j}\left[\frac{2\pi m}{l^*}-\frac{\omega}{v}\right]\Pi_m^*(\omega)-\rho A\omega^2. \tag{18}$$

$\Pi_m^*(\omega)$ in the latter equation is given as:

$$\Pi_m^*(\omega)=\frac{\kappa AG.\mathrm{j}\left[\frac{2\pi m}{l^*}-\frac{\omega}{v}\right]}{\kappa AG+EI\left[\frac{2\pi m}{l^*}-\frac{\omega}{v}\right]^2-\rho I\omega^2}. \tag{19}$$

In order to express the interaction force between the rail and the *i*th support in the frequency domain, i.e. $\hat{R}_i(\omega)$, as a function of the unknown coefficients of the rail displacement, one can take the Fourier transform of Eq. (6) and derive the following equation:

$$\hat{R}_i(\omega)=G_i(\omega)\hat{w}_{\mathrm{b}}(il_{\mathrm{s}},\omega), \tag{20}$$

in which the function $G_i(\omega)$ is defined as:

$$G_i(\omega)=\frac{\left(\mathrm{j}\omega c_{\mathrm{p},i}+k_{\mathrm{p},i}\right)\left(-\omega^2M_{\mathrm{s},i}+\mathrm{j}\omega c_{\mathrm{b},i}+k_{\mathrm{b},i}\right)}{-\omega^2M_{\mathrm{s},i}+\mathrm{j}\omega(c_{\mathrm{p},i}+c_{\mathrm{b},i})+(k_{\mathrm{p},i}+k_{\mathrm{b},i})}. \tag{21}$$

Eq. (11) can be substituted into Eq. (20) and finally the *i*th support/rail interaction force can be expressed in terms of the unknown amplitudes of the rail response, as follows:

$$\hat{R}_i(\omega)=\sum_{m=-\infty}^{+\infty}G_i(\omega)\bar{W}_m(\omega)\mathrm{e}^{\mathrm{j}(\frac{2\pi m}{l^*}-\frac{\omega}{v})il_{\mathrm{s}}}. \tag{22}$$

Substituting the interaction force obtained in the latter equation into Eq. (17) yields:

$$\sum_{m=-\infty}^{+\infty}\left\{\bar{W}_m(\omega)\left[\Lambda_m^*(\omega)\mathrm{e}^{\mathrm{j}(\frac{2\pi m}{l^*}-\frac{\omega}{v})x}+\sum_{i=-\infty}^{+\infty}G_i(\omega)\delta(x-il_{\mathrm{s}})\mathrm{e}^{\mathrm{j}(\frac{2\pi m}{l^*}-\frac{\omega}{v})il_{\mathrm{s}}}\right]+\frac{\bar{F}_m}{v}\mathrm{e}^{\mathrm{j}(\frac{2\pi m}{l^*}-\frac{\omega}{v})x}\right\}=0. \tag{23}$$

Since a Dirac comb (infinite series of Dirac delta functions) is a sampling function extracting samples from a continuous signal, Eq. (23) can be rewritten as follows:

$$\sum_{m=-\infty}^{+\infty}\left\{\bar{W}_m(\omega)\left[\Lambda_m^*(\omega)\mathrm{e}^{\mathrm{j}(\frac{2\pi m}{l^*}-\frac{\omega}{v})x}+\mathrm{e}^{\mathrm{j}(-\frac{\omega}{v})x}\sum_{i=-\infty}^{+\infty}G_i(\omega)\delta(x-il_s)\mathrm{e}^{\mathrm{j}(\frac{2\pi m}{l^*})il_s}\right]+\frac{\bar{F}_m}{v}\mathrm{e}^{\mathrm{j}(\frac{2\pi m}{l^*}-\frac{\omega}{v})x}\right\}=0. \tag{24}$$

The Dirac comb in the latter equation is a periodic function with period l^*, accordingly expressed as a Fourier series. Therefore, Eq. (24) can be rewritten again and the following equation can be found:

$$\sum_{m=-\infty}^{+\infty}\left\{\bar{W}_m(\omega)\left[\Lambda_m^*(\omega)\mathrm{e}^{\mathrm{j}\left(\frac{2\pi m}{l^*}\right)x}+\frac{1}{l^*}\sum_{n=-\infty}^{+\infty}\sum_{i=0}^{N_1+N_2+N_3-1}G_i(\omega)\mathrm{e}^{\mathrm{j}\left(\frac{2\pi n}{l^*}\right)x}\mathrm{e}^{-\mathrm{j}\left(\frac{2\pi(n-m)}{l^*}\right)il_s}\right]+\frac{\bar{F}_m}{v}\mathrm{e}^{\mathrm{j}\left(\frac{2\pi m}{l^*}\right)x}\right\}=0. \tag{25}$$

Taking into account $2N_t+1$ terms of the infinite series in Eq. (25) and using linear independence of the exponential functions, a set of algebraic equations (given in a matrix form) is found:

$$\mathbf{CO}_{(2N_t+1)\times(2N_t+1)}\bar{\mathbf{W}}_{(2N_t+1)\times1}=-\frac{1}{v}\bar{\mathbf{F}}_{(2N_t+1)\times1}, \tag{26}$$

where $\mathbf{CO}$, $\bar{\mathbf{W}}$ and $\bar{\mathbf{F}}$ are given as:

$$\mathbf{CO}=\begin{bmatrix}\Lambda_{-N_t}^*+\frac{1}{l^*}\sum_{i=0}^{N_1+N_2+N_3-1}G_i & \frac{1}{l^*}\sum_{i=0}^{N_1+N_2+N_3-1}G_i\mathrm{e}^{\mathrm{j}\frac{2\pi il_s}{l^*}} & \frac{1}{l^*}\sum_{i=0}^{N_1+N_2+N_3-1}G_i\mathrm{e}^{\mathrm{j}\frac{2\pi il_s(2)}{l^*}} & \cdots & \frac{1}{l^*}\sum_{i=0}^{N_1+N_2+N_3-1}G_i\mathrm{e}^{\mathrm{j}\frac{2\pi il_s(2N_t)}{l^*}}\\ \frac{1}{l^*}\sum_{i=0}^{N_1+N_2+N_3-1}G_i\mathrm{e}^{-\mathrm{j}\frac{2\pi il_s}{l^*}} & \Lambda_{-N_t+1}^*+\frac{1}{l^*}\sum_{i=0}^{N_1+N_2+N_3-1}G_i & \frac{1}{l^*}\sum_{i=0}^{N_1+N_2+N_3-1}G_i\mathrm{e}^{\mathrm{j}\frac{2\pi il_s}{l^*}} & \cdots & \frac{1}{l^*}\sum_{i=0}^{N_1+N_2+N_3-1}G_i\mathrm{e}^{\mathrm{j}\frac{2\pi il_s(2N_t-1)}{l^*}}\\ \vdots & \vdots & \vdots & \ddots & \vdots\\ \frac{1}{l^*}\sum_{i=0}^{N_1+N_2+N_3-1}G_i\mathrm{e}^{-\mathrm{j}\frac{2\pi il_s(2N_t)}{l^*}} & \frac{1}{l^*}\sum_{i=0}^{N_1+N_2+N_3-1}G_i\mathrm{e}^{-\mathrm{j}\frac{2\pi il_s(2N_t-1)}{l^*}} & \cdots & \frac{1}{l^*}\sum_{i=0}^{N_1+N_2+N_3-1}G_i\mathrm{e}^{-\mathrm{j}\frac{2\pi il_s}{l^*}} & \Lambda_{N_t}^*+\frac{1}{l^*}\sum_{i=0}^{N_1+N_2+N_3-1}G_i\end{bmatrix}, \tag{27}$$

$$\bar{\mathbf{W}}=\begin{Bmatrix}\bar{W}_{-N_t}(\omega)\\ \bar{W}_{-N_t+1}(\omega)\\ \vdots\\ \bar{W}_0(\omega)\\ \bar{W}_1(\omega)\\ \vdots\\ \bar{W}_{N_t}(\omega)\end{Bmatrix},\quad \bar{\mathbf{F}}=\begin{Bmatrix}\bar{F}_{-N_t}\\ \bar{F}_{-N_t+1}\\ \vdots\\ \bar{F}_0\\ \bar{F}_1\\ \vdots\\ \bar{F}_{N_t}\end{Bmatrix}. \tag{28}$$

Eq. (26) can now be employed to relate the unknown amplituds of the rail displacement to the unknown coefficients of the wheel/rail contact force. This can be carried out by introducing the following matrix,

$$\boldsymbol{\Theta}(\omega)=\begin{bmatrix} \Theta_{1,1} & \Theta_{1,2} & \cdots & \Theta_{1,2N_t+1} \\ \Theta_{2,1} & \Theta_{2,2} & \cdots & \Theta_{2,2N_t+1} \\ \vdots & \vdots & \vdots & \vdots \\ \Theta_{2N_t+1,1} & \Theta_{2N_t+1,2} & \cdots & \Theta_{2N_t+1,2N_t+1} \end{bmatrix} = \mathbf{C}\mathbf{O}^{-1}, \tag{29}$$

and using the following relationship:

$$\bar{W}_m(\omega) = -\frac{1}{v}\sum_{n=-N_t}^{N_t} \Theta_{m+(N_t+1),n+(N_t+1)}\bar{F}_n\,, \quad m=-N_t,...,N_t. \tag{30}$$

The latter equation is substituted into Eq. (11) in order to find the rail displacement in the frequency domain, as a function of the unknown coefficients of the contact force:

$$\hat{w}_b(x,\omega) = -\frac{1}{v}\mathrm{e}^{-\mathrm{j}\omega x/v}\sum_{m=-N_t}^{N_t}\sum_{n=-N_t}^{N_t} \Theta_{m+(N_t+1),n+(N_t+1)}\bar{F}_n\ \mathrm{e}^{\mathrm{j}m(\frac{2\pi}{l^*})x}. \tag{31}$$

The rail response in the time domain can now be obtained by taking the inverse Fourier transform of both sides of Eq. (31):

$$w_b(x,t) = -\frac{1}{v}\sum_{m=-N_t}^{N_t}\sum_{n=-N_t}^{N_t} \theta_{m+(N_t+1),n+(N_t+1)}(t-x/v)\bar{F}_n\ \mathrm{e}^{\mathrm{j}m(\frac{2\pi}{l^*})x}, \tag{32}$$

in which $\theta_{i,j}(t)$ is defined as:

$$\theta_{i,j}(t) = \frac{1}{2\pi}\int_{-\infty}^{+\infty} \Theta_{i,j}\,\mathrm{e}^{\mathrm{j}\omega t}d\omega, \quad i,j=1,2,...,2N_t+1. \tag{33}$$

Derivation of the wheel response in terms of the contact force amplitudes can be carried out by substituting the contact force (Eq. (8)) and the rail response (Eq. (32)) into Eq. (2), resulting in the following mathematical expression:

$$w_w(t) = -\sum_{m=-N_t}^{N_t}\left[\frac{\bar{F}_m}{k_H}+\frac{1}{v}\sum_{n=-N_t}^{N_t}\theta_{m+(N_t+1),n+(N_t+1)}(0)\bar{F}_n\right]\mathrm{e}^{\mathrm{j}m(\frac{2\pi v}{l^*})t}. \tag{34}$$

The contact force and the wheel response, derived in Eqs. (8) and (34), are used in Eq. (1) in order to obtain the following set of algebraic equations containing the unknown amplitudes of the contact force:

$$m_w\left(\frac{2\pi m v}{l^*}\right)^2\left[\frac{\bar{F}_m}{k_H}+\frac{1}{v}\sum_{n=-N_t}^{N_t}\theta_{m+(N_t+1),n+(N_t+1)}(0)\bar{F}_n\right] = \bar{F}_m, \ m=-N_t,...,N_t, \ m\neq 0. \tag{35}$$

It is worth noting that the wheel/rail interaction force component corresponding to $m=0$ is equal to the static wheel load, i.e. $\bar{F}_0 = -m_{tot}g$. The latter equation can be rewritten in a matrix form:

$$\mathbf{H}_{2N_t\times 2N_t}\bar{\mathbf{f}}_{2N_t\times 1} = \frac{-\bar{F}_0}{v}\boldsymbol{\theta}^*_{2N_t\times 1}, \tag{36}$$

in which $\mathbf{H}$, $\bar{\mathbf{f}}$ and $\boldsymbol{\theta}^*$ are given as:

$$\mathbf{H}=\begin{bmatrix} h_{1,1} & h_{1,2} & \cdots & h_{1,N_t} & h_{1,N_t+2} & h_{1,N_t+3} & \cdots & h_{1,2N_t+1} \\ h_{2,1} & h_{2,2} & \cdots & h_{2,N_t} & h_{2,N_t+2} & h_{2,N_t+3} & \cdots & h_{2,2N_t+1} \\ \vdots & \vdots & \ddots & \vdots & \vdots & \vdots & \vdots & \vdots \\ h_{N_t,1} & h_{N_t,2} & \cdots & h_{N_t,N_t} & h_{N_t,N_t+2} & h_{N_t,N_t+3} & \cdots & h_{N_t,2N_t+1} \\ h_{N_t+2,1} & h_{N_t+2,2} & \cdots & h_{N_t+2,N_t} & h_{N_t+2,N_t+2} & h_{N_t+2,N_t+3} & \cdots & h_{N_t+2,2N_t+1} \\ h_{N_t+3,1} & h_{N_t+3,2} & \cdots & h_{N_t+3,N_t} & h_{N_t+3,N_t+2} & h_{N_t+3,N_t+3} & \cdots & h_{N_t+3,2N_t+1} \\ \vdots & \vdots & \vdots & \vdots & \vdots & \vdots & \ddots & \vdots \\ h_{2N_t+1,1} & h_{2N_t+1,2} & \cdots & h_{2N_t+1,N_t} & h_{2N_t+1,N_t+2} & h_{2N_t+1,N_t+3} & \cdots & h_{2N_t+1,2N_t+1} \end{bmatrix}, \tag{37}$$

$$\bar{\mathbf{f}}=\begin{bmatrix} \bar{F}_{-N_t} \\ \bar{F}_{-N_t+1} \\ \vdots \\ \bar{F}_{-1} \\ \bar{F}_{1} \\ \bar{F}_{2} \\ \vdots \\ \bar{F}_{N_t} \end{bmatrix}, \quad \boldsymbol{\theta}^*=\begin{bmatrix} \theta_{1,N_t+1}(0) \\ \theta_{2,N_t+1}(0) \\ \vdots \\ \theta_{N_t,N_t+1}(0) \\ \theta_{N_t+2,N_t+1}(0) \\ \theta_{N_t+3,N_t+1}(0) \\ \vdots \\ \theta_{2N_t+1,N_t+1}(0) \end{bmatrix}. \tag{38}$$

Moreover, the elements of $\mathbf{H}$ are defined in the following equation:

$$\begin{cases} h_{m,n}=\dfrac{1}{k_{\mathrm{H}}}-\dfrac{l^{*2}}{m_{\mathrm{w}}\left(2\pi v(m-N_{\mathrm{t}}-1)\right)^2}+\dfrac{\theta_{m,n}(0)}{v} & \text{If } m=n \\ h_{m,n}=\dfrac{\theta_{m,n}(0)}{v} & \text{If } m\neq n \end{cases}. \tag{39}$$

The unknown coefficients of the contact force can now be obtained from Eq. (36):

$$\bar{\mathbf{f}}_{2N_t\times 1}=\frac{m_{\mathrm{tot}}g}{v}\mathbf{H}^{-1}_{2N_t\times 2N_t}\boldsymbol{\theta}^*_{2N_t\times 1}. \tag{40}$$

The amplitudes of the contact force obtained from the latter equation are used in Eq. (32) in order to find the time-domain response of the track with varying support stiffness to the moving unsprung mass.

The substructure being represented by Kelvin-Voigt elements under the individual sleepers, the energy dissipation can now be derived from the dynamic sleeper response. The response of the *i*th sleeper in the frequency domain can be obtained first by taking the Fourier transform of both sides of the equation of

motion for the *i*th sleeper (see Eq. (6)) and then employing the *i*th rail/sleeper interaction force derived in Eq. (20). The velocity response in the frequency domain is derived as follows:

$$\hat{v}_{\mathrm{s},i}(\omega) = \mathrm{j}\omega\,\hat{w}_{\mathrm{s},i}(\omega) = \frac{\mathrm{j}\omega\left(\mathrm{j}\omega c_{\mathrm{p},i} + k_{\mathrm{p},i}\right)}{-\omega^2 M_{\mathrm{s},i} + \mathrm{j}\omega(c_{\mathrm{p},i} + c_{\mathrm{b},i}) + (k_{\mathrm{p},i} + k_{\mathrm{b},i})}\,\hat{w}_{\mathrm{b}}(il_{\mathrm{s}}, \omega), \tag{41}$$

in which the frequency response of the rail at $x = il_{\mathrm{s}}$, i.e. $\hat{w}_{\mathrm{b}}(il_{\mathrm{s}}, \omega)$, is given in Eq. (31). Employing the latter equation, the mechanical energy dissipated by the substructure/ballast damping in the *i*th support can be obtained:

$$E_{\mathrm{diss},i} = \int_{-\infty}^{+\infty} f_{\mathrm{d},i}(t) v_{\mathrm{s},i}(t)\,dt = \int_{-\infty}^{+\infty} c_{\mathrm{b},i} v_{\mathrm{s},i}(t)^2\,dt, \tag{42}$$

where $v_{\mathrm{s},i}(t)$ is the velocity response of the *i*th sleeper in the time domain obtained by taking the inverse Fourier transform of the frequency response in Eq. (41).

3. Parametric study of local non-uniformity in the track support

This section provides and discusses simulation results for case *i* - degrading individual sleeper support - as defined in the introduction. It is structured as follows: paragraph 3.1. specifies parameter input; 3.2. discusses model convergence criteria; 3.3 discusses the description of the expected degradation in terms of energy dissipation and its benchmarking; 3.4 discusses simulations concerning effects of the degree of local non-uniformity; 3.5 provides a full parametric analysis of the system parameters in the presence of support non-uniformity, and 3.6 discusses the potential of the developed methodology for system optimization in view of life-cycle performance.

3.1 Parameter input

In analogy to the approach taken in [1], the nominal, lower and upper values of wheel/track parameters are used as shown in Table 1; they represent the nominal values characteristic for Dutch track. For each parameter, lower and upper limits are assigned. A static wheel load of 100 kN, and a shear coefficient (κ) of 0.34 [25] are used in the simulations, and the linearized contact stiffness (k_{H}) is calculated as $\sqrt[3]{3\times10^{22}\cdot Q}$, with *Q* the static wheel load [26].

Table 1. Values of the input parameters of the model used in the parametric study [1]

Parameters	Lower value	Nominal value	Upper value
Rail			
Bending stiffness (*EI*), MNm^2	-	4.25 (54E1 profile)	6.11 (60E1)
Mass per length (ρA), kgm^{-1}	-	54.4 (54E1 profile)	60.34 (60E1)
Sleeper			
Sleeper mass (M_s), kg	50	142.5	202
Distance between sleepers (l_s), m	0.5	0.6	0.7

Pads			
Pad stiffness (k_p), MNm^{-1}	30	200	1000*
Pad damping (c_p), kNm^{-1}s	20	30	-
Ballast			
Ballast stiffness (k_b), MNm^{-1}	40	50	60
Ballast damping (c_b), kNm^{-1}s	-	55	-
Moving wheel			
Speed (km/h)	0	-	300
Unsprung mass (kg)	600	900	1200

* The pad stiffness of 1000 MN/m corresponds to the Corkelast pad used for typical Dutch track

An important assumption in this study, which concentrates on variation of the ballast/subgrade stiffness, concerns the corresponding damping value. As is also clear from Eqs. (41) and (42), the energy dissipation depends on the choice of this damping. Although in parametric analysis it is common to change only one parameter a time, a relationship between stiffness and damping levels cannot be excluded in this case. Only very few measurements are available in the scientific literature, all of them aiming at establishing some level for uniform track; a potential correlation between stiffness variation and damping variation has not been reported. Also from a theoretical viewpoint it is hard to assume or establish such a relationship, because there is no uniform view on the most appropriate description of the damping type. In this work, a constant damping-stiffness ratio is set as a default; besides, results assuming a uniform (and therefore uncoupled) damping value in space will be shown in comparison in the benchmark with the uniform track case (discussed in [1]) to illustrate the difference.

3.2 Model convergence

In the case of a degraded sleeper support or an unsupported (hanging) sleeper, N_2 is equal to 1, meaning that $N_1 + N_3$ identical supports with stiffness $k_{\mathrm{b},1}$ and one degraded support with stiffness $k_{\mathrm{b},0}$ are considered in the wheel/track model in Fig. 2. To obtain sufficiently accurate results, the minimum number of sleepers in subsections N_1 (denoted as $N_{1\min}$) and N_3 (denoted as $N_{3\min}$) and the total number of sections (NOS) must be calibrated. As a convergence criterion the condition is chosen that both the influence of the non-uniformity vanishes in space and the local energy dissipation level at both extremities of N_e are equal to that of the adjacent uniform track, where N_e represents the total area influenced by the non-uniformity. This is ensured by appropriate choices of $N_{1\min}$ and $N_{3\min}$, whereas NOS guarantees a sufficient frequency range. The convergence depends on all system parameters and the train speed. An example of the convergence check is given in **Error! Reference source not found.**, showing the spatial distribution of energy dissipation along the supports for v = 300 km/h and nominal parameter values, implying $k_{\mathrm{b},1}$ equals 50 MN/m. The stiffness ratio r is chosen as $r = k_{\mathrm{b},0}/k_{\mathrm{b},1} = 0.25$. The energy dissipation of a uniform track is shown as a reference. For the case of **Error! Reference source not found.**, the choice of $N_1 = 7$, $N_3 = 25$ and NOS = 9 leads to convergent results.

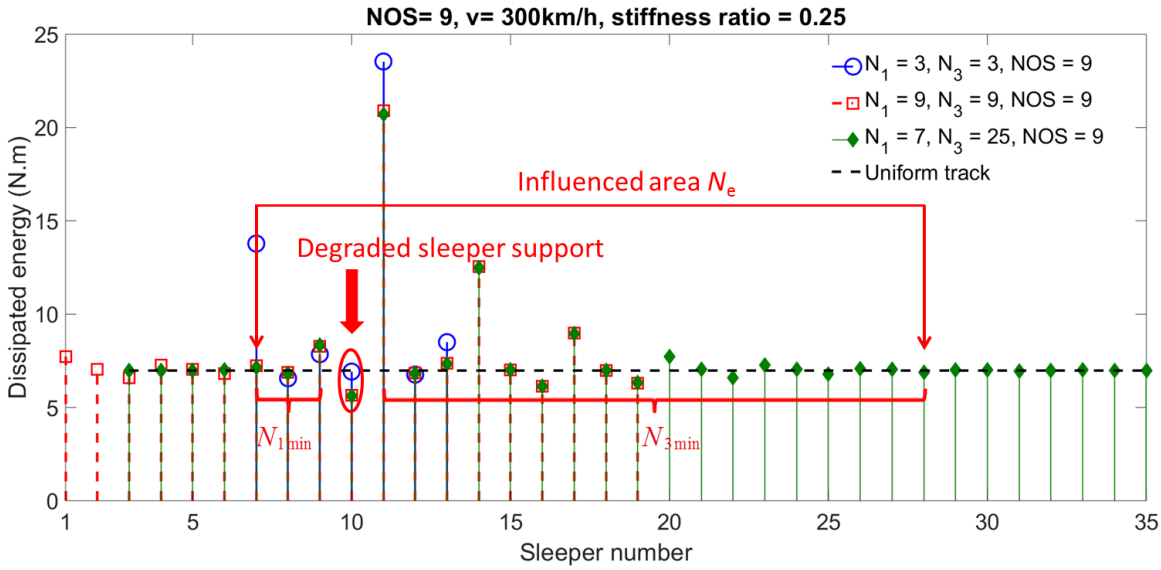

(a) Convergence check for N_1 and N_3

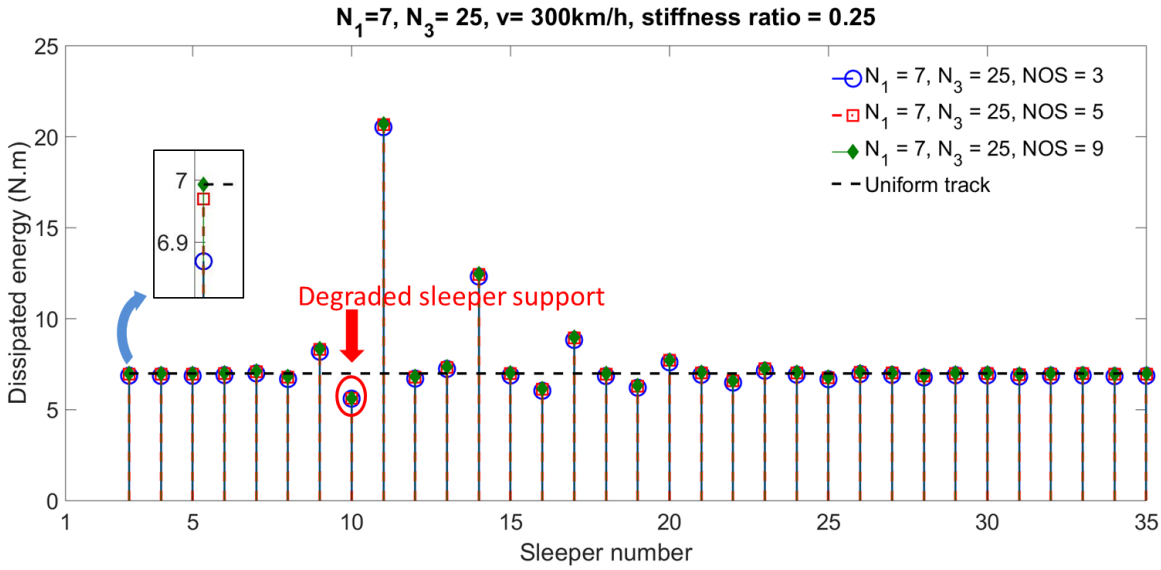

(b) Convergence check for NOS

Fig. 3. Convergence of the model for nominal parameter values and v=300km/h

3.3 Description of the expected degradation in terms of energy dissipation and benchmarking

There is no standardized measure to describe the expected degradation rate, in terms of energy dissipation, for track non-uniformity, in this case for a hanging sleeper. Given the fact that only differential dissipation at different supports can lead to differential settlement and a deteriorating geometry, this study proposes four possible measures or indicators that seem, a priori, appropriate:

(a) the root mean square (RMS) of energy dissipation in the influenced area N_e;

(b) the RMS of differential energy dissipation (denoted as RMS(DD)) in the influenced area N_e;

(c) the maximum differential dissipation (denoted as MDD) between adjacent sleepers over the entire influenced area N_e;

(d) the differential dissipation in absolute sense (denoted as DD) between the degraded sleeper and the following sleeper (which is therefore a localised measure).

The RMS of energy dissipation for a given amount of sleepers (measure (a)) is the expected value of the dissipation over the corresponding non-uniform track section, which at the same time accounts for the 'intensity' of the non-uniformity over this section. It can be determined by finding the mechanical energy dissipation in each support (see Eq. (42)), and then calculating the following parameter:

$$E_{\text{diss,rms}} = \sqrt{\frac{1}{N_e}\sum_{i=1}^{N_e} E_{\text{diss},i}^2}\ . \tag{43}$$

For a single passage of the moving unsprung mass, MDD (measure (c)) can be calculated from:

$$\text{MDD} = \max|\boldsymbol{\varepsilon}|, \tag{44}$$

in which $|.|$ denotes absolute value. $\boldsymbol{\varepsilon}$ is a vector with $N_1 + N_2 + N_3 - 1$ elements, and the ith element of this vector is given below:

$$DD_i = \varepsilon_i = E_{\text{diss},i+1} - E_{\text{diss},i},\ i = 1,2,...,N_1 + N_2 + N_3 - 1. \tag{45}$$

Expressed differently, MDD is the largest element of $|\boldsymbol{\varepsilon}|$. By checking MDD and its position, one can localise the degradation "hotspot".

The root mean square of differential energy dissipation in the influenced area N_e (measure (b)) can be calculated as

$$DD_{\text{rms}} = \sqrt{\frac{1}{N_e}\sum_{i=1}^{N_e} \varepsilon_i^2} \tag{46}$$

The difference of energy dissipation between the degraded sleeper and the following sleeper (measure (d)) is basically the (N_1+1)th element of $\boldsymbol{\varepsilon}$, namely DD_{N_1+1}.

By setting the stiffness ratio r = 1, the developed model reduces into the one employed in [1] and therefore this model can also deal with uniform track case. Fig. 4(a) reproduces the energy dissipation of such uniform track with nominal system values according to Table 1 and a wide range of ballast/soil stiffness values, whereas Fig. 4(b-e) shows the results, for a single degraded sleeper with r = 0.75, in terms of the previously proposed measures Eqs. (43-46), and assuming, for this comparison, a constant damping. The comparison shows that (a) all measures have qualitatively very similar trends, except DD, and (b) these

trends are similar for uniform track and non-uniform track with a hanging sleeper; qualitatively for the RMS(DD) and MDD descriptions, and quantitatively for the RMS description - due to its averaging effect. An important further observation is that the differential dissipation between the degraded sleeper support and its neighbor is not always the largest occurring within the influence zone, explaining the difference between MDD and DD (in absolute sense); in fact, the position of MDD varies within the N_e area. It may be concluded that all descriptions are somehow appropriate, with DD providing however only very local information. Peaks are found at speeds when the sleeper passing frequency (i.e. v/l_s) coincides with the first resonance peak in the receptance function of the wheel/track model. Finally, Fig. 4(f) illustrates the effect of the chosen constant ballast damping value on the behavior of the MDD description as a function of the train speed, for one specific track stiffness, $k_{b,1} = 100\text{MNm}^{-1}$; the nominal damping value is increased with a theoretical factor 2 and 4. An obvious result is that higher overall damping results in a higher MDD level in absolute sense. However, this simulation also shows a second aspect which is more relevant: both the height and the position of the dissipation peak are affected by the damping value; a higher damping leads to a significantly decreasing peak value whereas the corresponding speed shifts slightly upward.

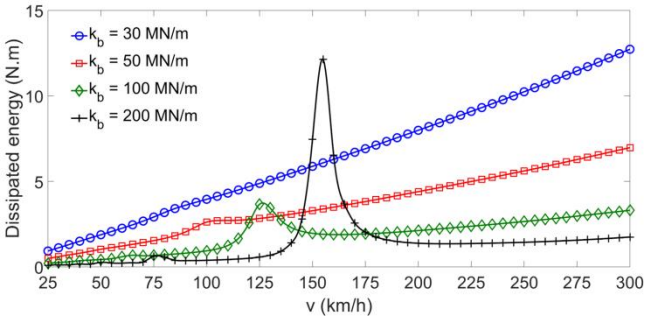

(a) Energy dissipation for r=1

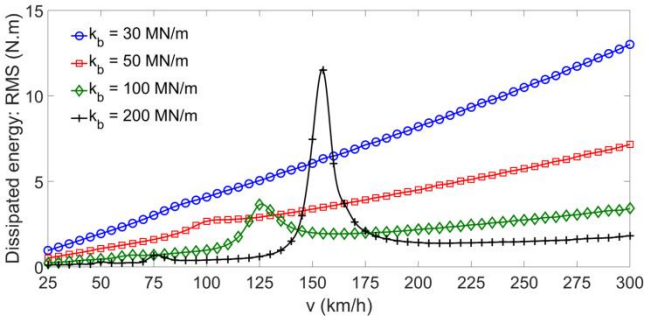

(b) RMS

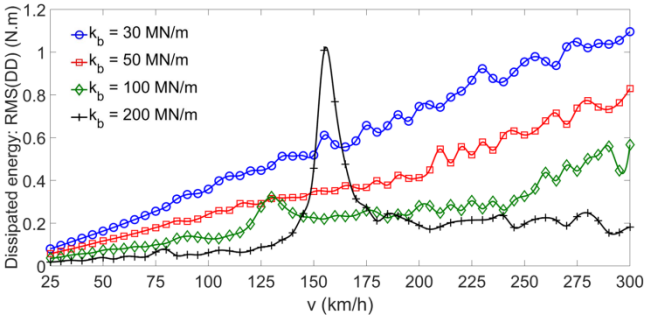

(c) RMS(DD)

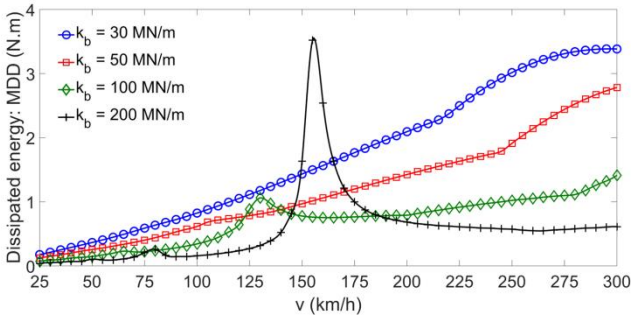

(d) MDD

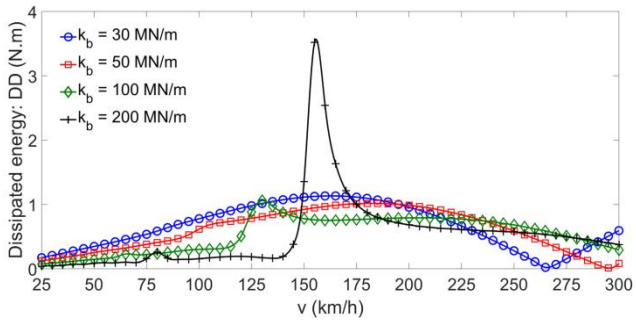

(e) DD

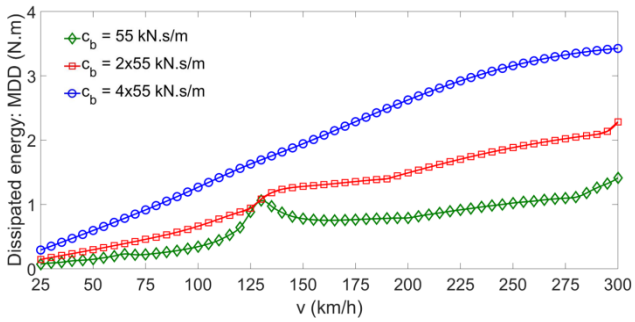

(f) influence of damping on MDD

Fig. 4. Effect of subgrade/ballast stiffness for stiffness ratio r ($k_{b,0}/k_{b,1} = 0.75$); constant subgrade damping

3.4 Effects of the degree of local non-uniformity

In order to investigate the effect of the level to which the sleeper support is affected, i.e. $r = k_{b,0}/k_{b,1}$, the measures (a-d) according to Eqs. (43-46) are computed at three different values of this ratio; 0.25, 0.5 and 0.75. Again, nominal values are used for wheel/track parameters. This time however, in contrast to the previous paragraph and Fig. 4, a constant damping ratio is used. It is defined as the ratio of the nominal values of the ballast stiffness and ballast damping, i.e. $k_b / c_b = 5\times10^7 / 5.5\times10^4$, hereafter designated as the nominal damping ratio. The obtained results are shown in Fig. 5. Comparison of the results in this figure shows that MDD and RMS(DD) have qualitatively almost identical trends; as can be expected however, quantitatively they differ with higher values for MDD. The overall RMS value also has a similar prediction, but differentiates less between the stiffness ratios. Further, DD shows a behavior comparable to MDD, suggesting a largely consistent occurrence of MDD at the adjacent sleeper when a constant damping ratio is assumed. It can be concluded that DD is most sensitive to the damping model choice, whereas MDD is both a more general and a more generally valid indicator for track degradation. Based on the previous, the indicators RMS (definition (a)) and MDD (definition (c)) are chosen for all further analyses in this study. Both measures grow with the train speed regardless of the stiffness ratio. Moreover, it can be concluded that the magnitude of the local stiffness variation (the stiffness ratio) has a very significant influence on the expected long-term degradation of both normal and high-speed tracks. This computational result matches with the practical experience that 'hanging sleepers' develop progressively very fast.

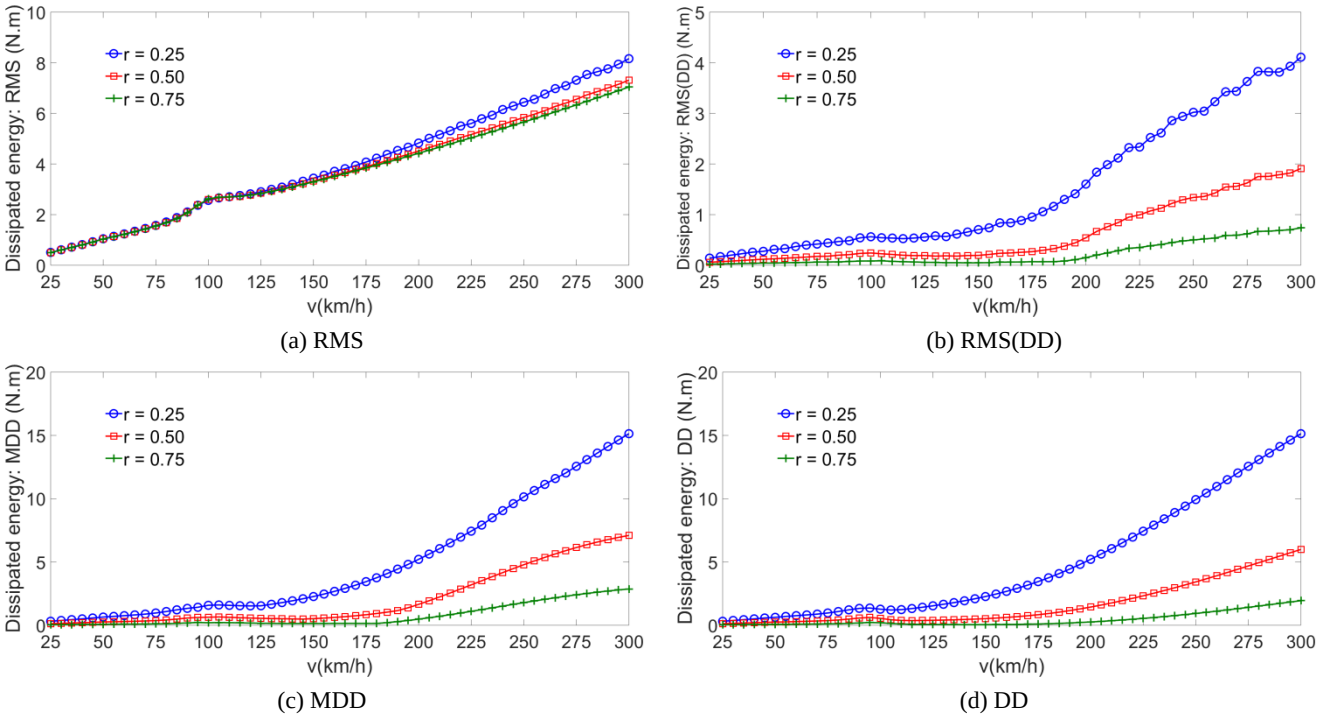

Fig. 5. Effect of the stiffness ratio r ($k_{b,0}/k_{b,1}$) for a degraded sleeper support on energy dissipation as a function of speed

Fig. 6 shows, in terms of RMS and MDD, the effect of the total number of adjacent degraded sleeper supports on the expected degradation, for different train speeds and a stiffness ratio r of 0.25. Whereas RMS provides little information in this case, it can be concluded from the MDD trend that the effect of an increasing number of adjacent degraded sleeper supports vanishes rather quickly; beyond a total number of 3 affected supports in series the effect is no longer significant for any speed.

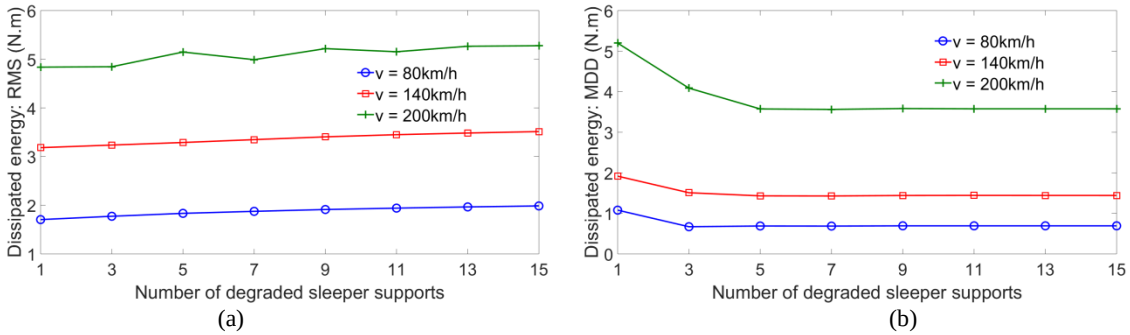

Fig. 6. Effect of number of degraded sleeper supports on energy dissipation ($r = k_{b,0}/k_{b,1} = 0.25$)

3.5 Full parametric investigation of all system design parameters

In this paragraph, a complete parametric study is carried out for all track design parameters, in analogy to the approach in [1], but now incorporating a degraded sleeper support and evaluating their effect on the expected degradation in terms of RMS and MDD. The constant and nominal ballast stiffness-damping ratio is used in the description of the non-uniformity. To examine the effect of each individual parameter, a bandwidth with lower and upper limits given in Table 1 is considered for the concerned parameter whereas nominal values are used for other parameters.

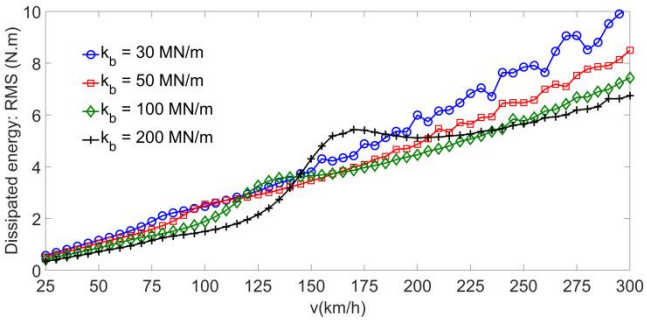

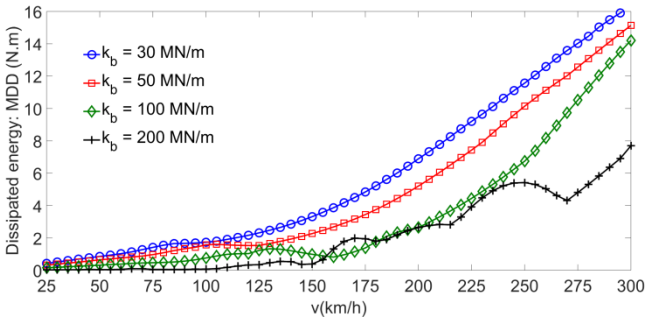

(a) stiffness ratio r=0.25, nominal damping ratio

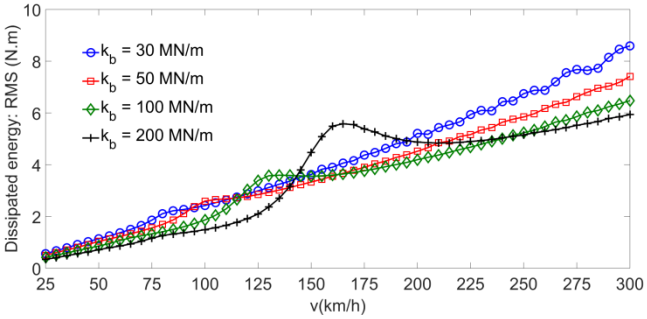

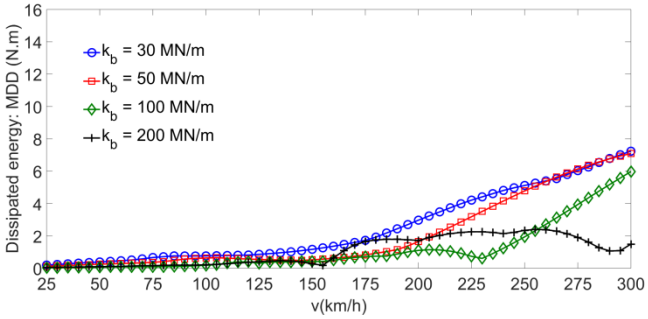

(b) stiffness ratio r=0.50, nominal damping ratio

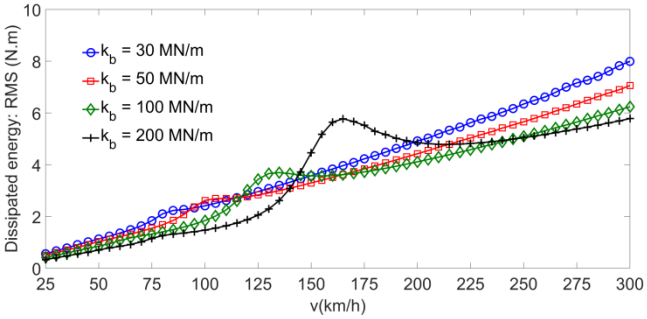

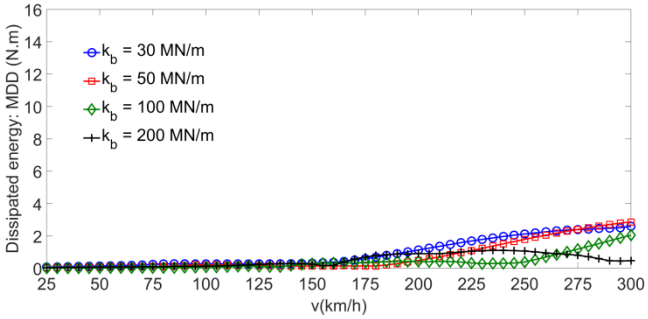

(c) stiffness ratio r=0.75, nominal damping ratio

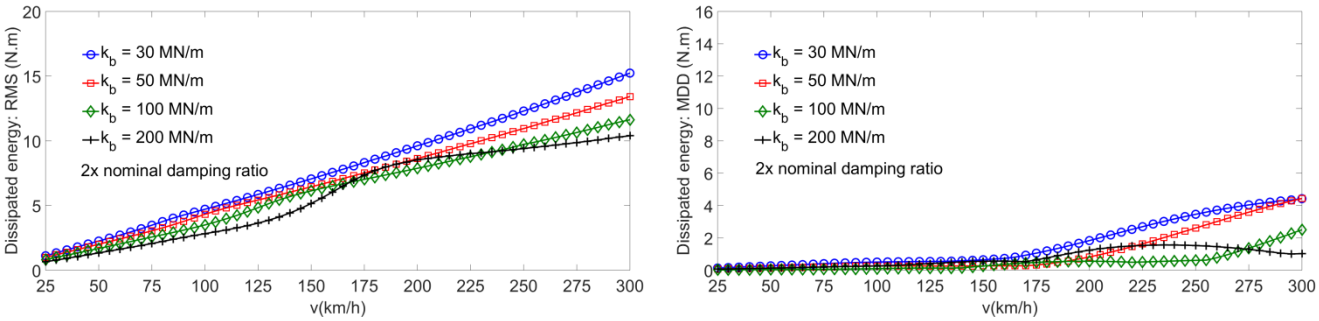

(d) stiffness ratio r=0.75, 2x (nominal damping ratio)

Fig. 7. Effect of subgrade/ballast stiffness on energy dissipation (left RMS, right MDD)

The most significant parameter affecting the long-term performance according to [1] was the subgrade/ballast stiffness. The effect of this stiffness is therefore investigated in detail, taking into account all three values of the stiffness ratio (r = 0.25, 0.50 and 0.75); results are shown in Fig. 7. In order to facilitate comparison of the charts for different r-values, the maximum of the vertical axes for the different cases have been taken identical in the series of graphs for both RMS and MDD respectively. Fig. 7 shows that the trend of RMS does not depend qualitatively on the stiffness ratio; due to the averaging effect, also quantitative predictions show little difference. The highest degradation level is expected for soft tracks in the entire speed domain, with a generally increasing trend of RMS with the speed. The peak in the speed domain occurs due to coincidence of the sleeper passing frequency (i.e. v/l_s) and the first resonance peak in the receptance function of the wheel/track model, identical to uniform track and explained in [1]. MDD does not suffer from the averaging effect of RMS; therefore the distinct peak does not occur here; moreover, the effect of a lower stiffness ratio on an increasing MDD is very clear. The effect of the subgrade stiffness is however roughly identical for both measures, indicating a consistently higher degradation rate on soft soils. Some of the graphs for MDD in Fig. 7 show a 'jerky' behavior, notably for higher subgrade stiffness; these 'jerks' correspond to speeds at which the position of MDD changes in space. Finally, Fig. 7(d) shows the effect of a varying damping ratio on the energy dissipation in the subgrade. Similar to the constant damping model, a larger damping ratio leads to diminishing sub-peaks at resonant speeds, while at the same time, as expected, increasing the overall energy dissipation. When comparing Fig. 7 and Fig. 4, it can be concluded that the ballast damping model (constant value versus constant ratio) is of significance for the obtained trends. The main conclusions however do not depend on the damping choice:

- the expected degradation increases globally with the speed;

- coincidence of the sleeper passing frequency with the first resonance peak of the system leads to severely increased degradation - the corresponding speed is within the operational window for conventional train operation;
- degradation concentrates on soft subgrades;
- a stronger local reduction of the stiffness (lower *r*-value) will lead to a higher degradation rate;
- increased damping diminishes dissipation peaks at resonant speeds and shifts their position to higher speeds.

Fig. 8 finally shows the effects of all system parameters on the energy dissipation (RMS and MDD) as a function of the train speed, for localized non-uniformity with r=0.25. Fig. 8(a) shows the railpad stiffness as a very significant parameter; especially for high-speed tracks a higher pad stiffness leads to both RMS and MDD values that are multiples of the values for a low pad stiffness. An increasing unsprung mass (Fig. 8(b)) is unfavorable for track degradation in terms of both RMS and especially MDD, with a special focus on high-speed track. Sleeper mass and railpad damping appear as rather irrelevant in Fig. 8(c,d). Both a shorter sleeper distance (Fig. 8(e)) and a stiffer rail profile (Fig. 8(f)) appear favorable for the long-term performance, again with the positive effect increasing with the train speed.

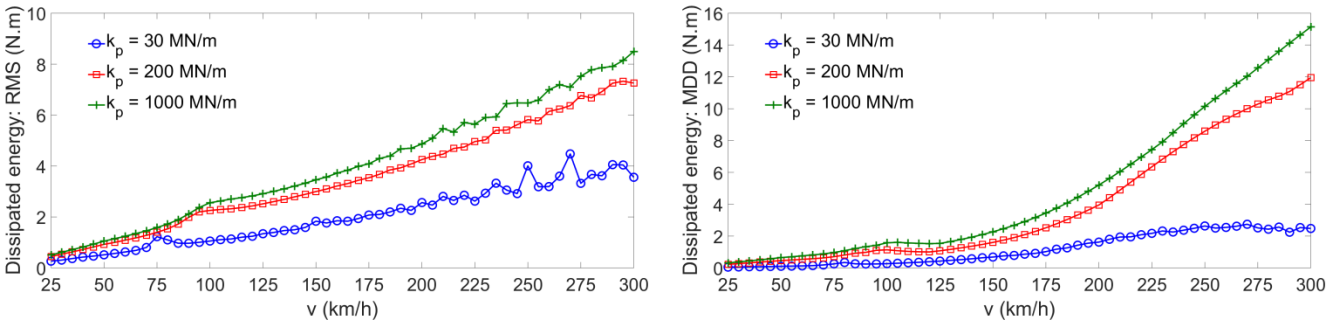

(a) Effect of railpad stiffness

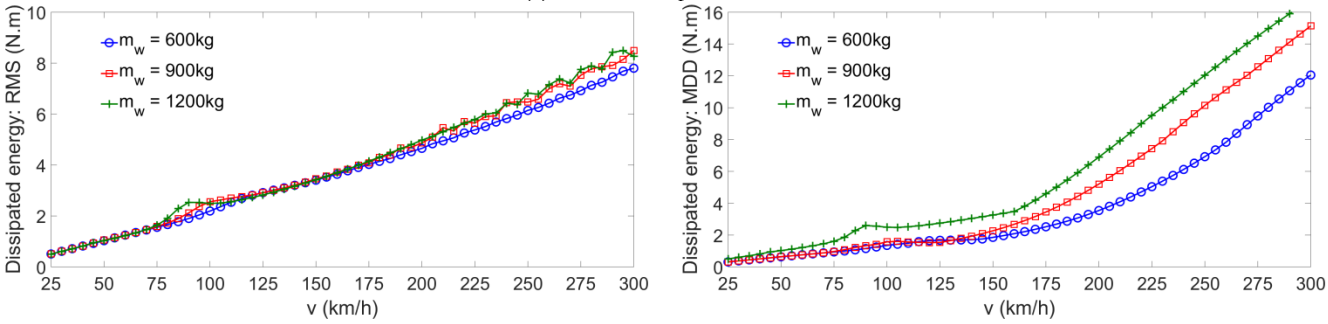

(b) Effect of unsprung mass

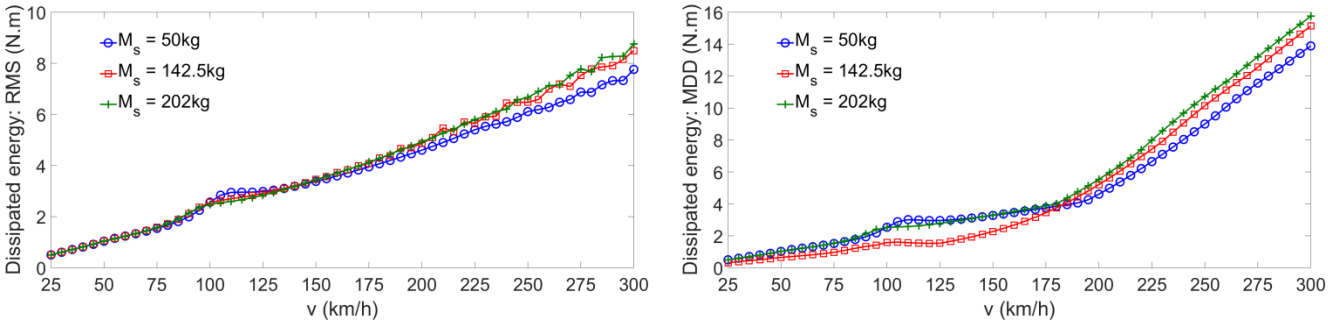

(c) Effect of sleeper mass

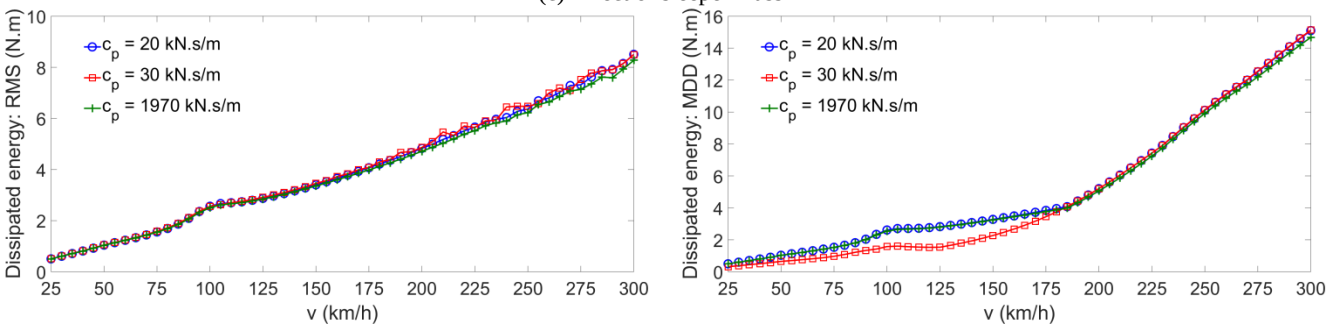

(d) Effect of railpad damping

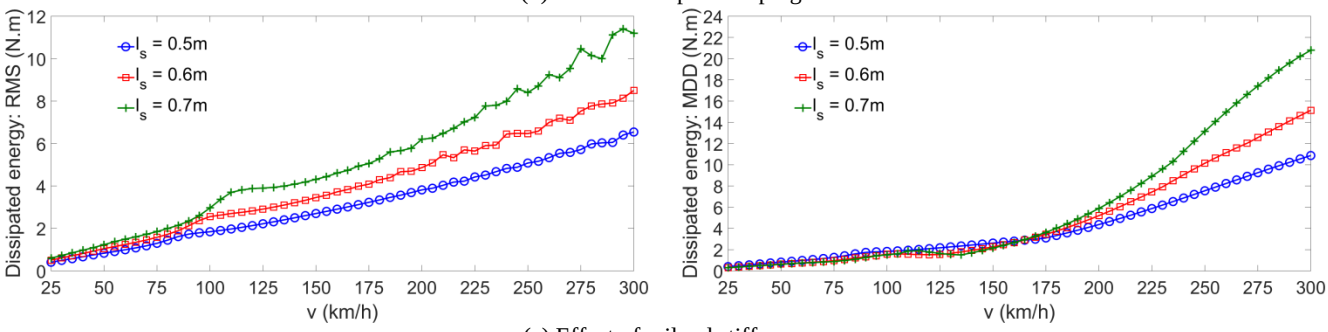

(e) Effect of railpad stiffness

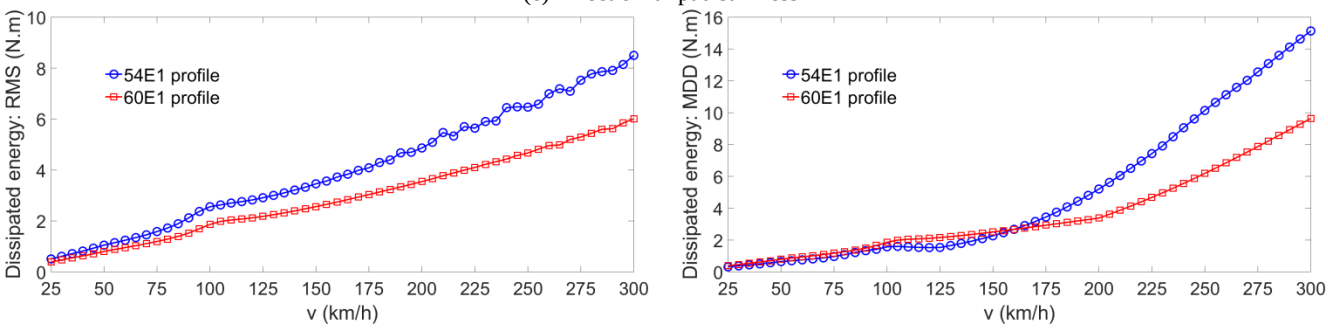

(f) Effect of rail profile

Fig. 8. Effects of various system parameters on energy dissipation for $r = k_{b,0} / k_{b,1} = 0.25$

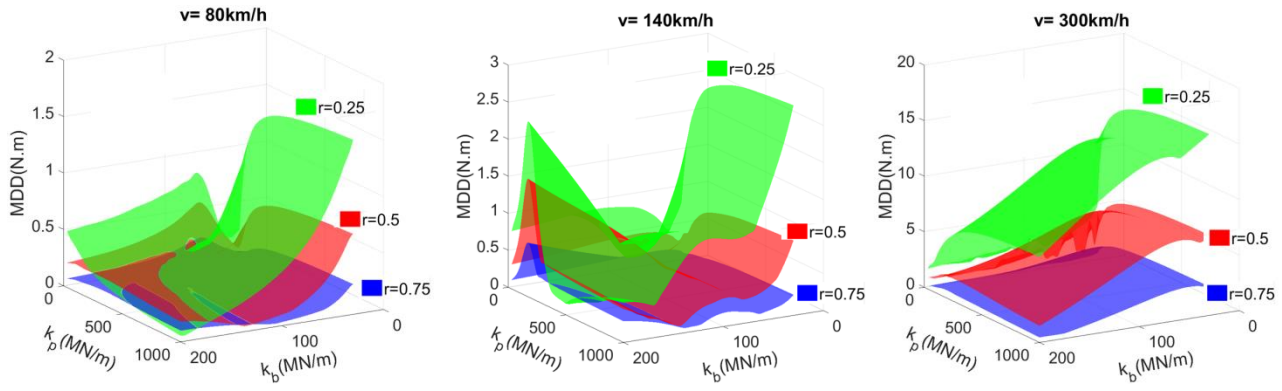

(a) (b) (c)

Fig. 9. 3D plot of dissipated energy for ballast stiffness range 30-200MNm^{-1} and railpad stiffness range 30-1000MNm^{-1} for three different velocities, in each figure $r = k_{b,0}/k_{b,1} = 0.25, 0.50, 0.75$ from the top to the bottom surface.

3.6 Potential of the method in track design

The developed methodology has significant potential with respect to railway track design, allowing also for multi-parametric optimization. In the previous paragraph, the sleeper distance and rail profile were found to be important parameters. For existing tracks however, often only the railpad stiffness is a parameter which can be adjusted rather easily. Fig. 9 shows, as an example, three-dimensional plots of MDD as a function of both substructure and ballast stiffness, for $r = 0.25$, 0.50 and 0.75. Three specific velocities are considered; 80 km/h for freight trains, 140 km/h for conventional passenger trains and 300 km/h for high-speed trains. The graphs show that the pad stiffness can be optimized independent of the severity of hanging sleepers but depending on the subgrade stiffness and the operational velocity; there is no unique value that satisfies all conditions.

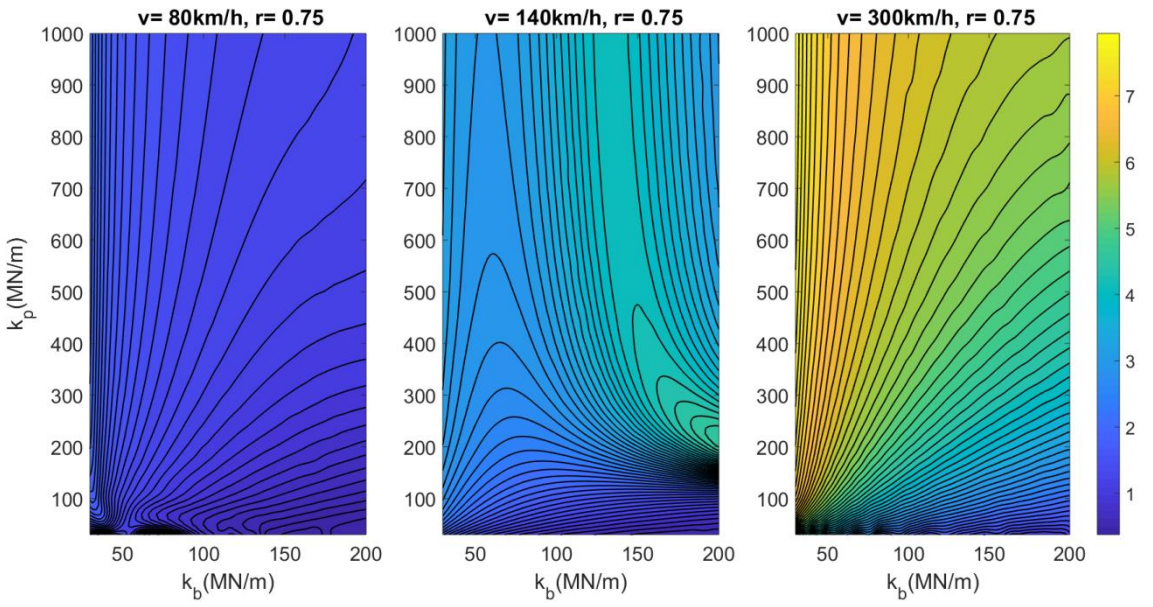

(a) RMS of energy dissipation in area N_e

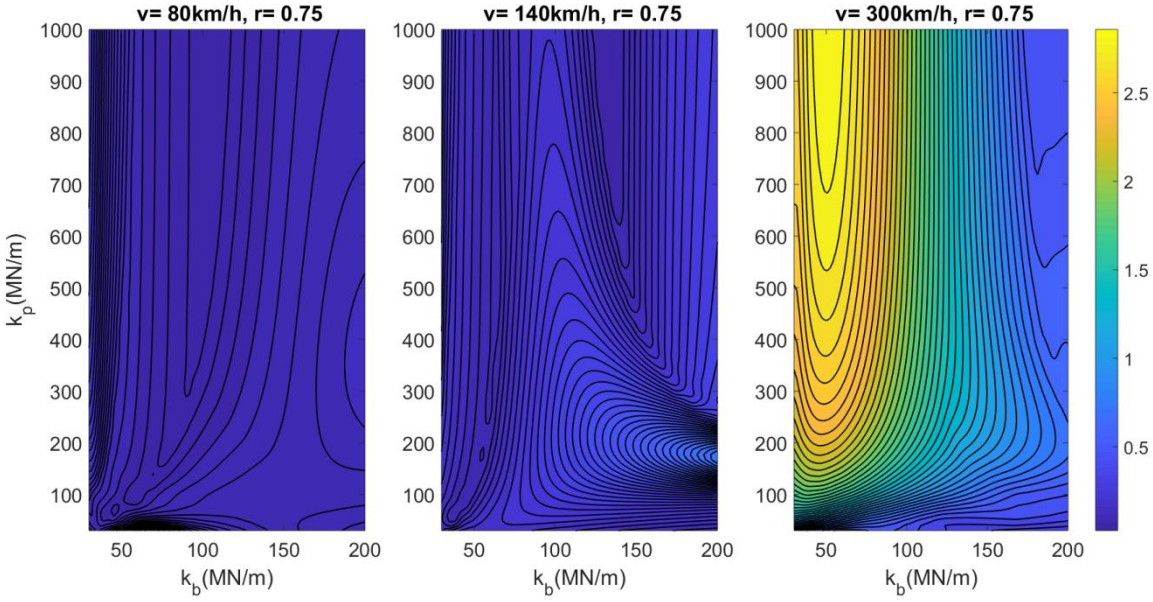

(b) MDD

Fig. 10. Contour plot of dissipated energy for ballast stiffness range 30-200MNm^{-1} and railpad stiffness range 30-1000MNm^{-1} for three different velocities and $r = k_{b,0}/k_{b,1} = 0.75$.

The optimization being independent on the stiffness ratio *r* of the non-uniformity, Fig. 10 shows for *r* = 0.75, again for the three operational train speeds an optimization with respect to the pad and the ballast/subgrade stiffness in terms of both RMS and MDD. The optimum pad stiffness can be easily

identified for each operational regime. A combination of low railpad and high track stiffness is preferred in many cases of track design.

4. Conclusions

This study addressed the contribution of spatial variance in the railway track support stiffness to the expected long-term track degradation, focusing on local variation in the form of a reduced sleeper support. A novel frequency-domain model has been developed with a double periodicity 'layer', capable of dealing with both sleeper periodicity and large-scale spatial variance in track properties. The susceptibility to degradation has been assessed by quantifying the mechanical energy dissipated in the substructure under a moving train axle. The study assumed a constant damping ratio in the description of the substructure non-uniformity and a viscous description of the energy loss. The spatial variability of the energy dissipated in the substructure is calculated as a measure to predict the expected track degradation rate, with the root mean square (RMS) of dissipated energy in the area which is influenced by the non-uniformity and the maximum differential dissipation (MDD) shown as appropriate indicators of expected degradation.

The work led to the following conclusions in particular, in the presence of a degraded sleeper support:

i. hanging sleepers develop faster with increasing train speed; the speed effect may be estimated - apart from eventual local resonance peaks - as roughly linear;

ii. the effect of the local stiffness reduction at the degraded support is very significant, with degradation increasing progressively with a higher relative stiffness reduction;

iii. degradation concentrates on soft subgrades;

iv. the effect of an increasing number of adjacent degraded sleeper supports vanishes after a total number of about 3 sleepers, for any train speed;

v. coincidence of the sleeper passing frequency with the first resonance peak of the system leads to severely increased degradation - the corresponding speed is within the operational window for conventional train operation;

vi. increased damping attenuates these dissipation peaks at resonant speeds and shifts their position to higher speeds;

vii. particularly the railpad stiffness is a very significant track design parameter; especially for high-speed tracks a higher pad stiffness leads to dissipation values that are multiples of the values for a low pad stiffness;

viii. whereas sleeper mass and railpad damping are irrelevant with respect to degradation, a shorter sleeper distance and a stiffer rail profile contribute to the long-term performance, again with the positive effect increasing with the train speed; for example, replacing a 54E1 with a 60E1 profile may reduce degradation with roughly 30% on high-speed track;

ix. an increasing unsprung vehicle mass is unfavorable for track degradation, with a special focus on high-speed track.

Finally, the potential of the developed methodology with respect to railway track design in terms of multi-parametric optimization was shown with the help of design charts. Generally speaking, a combination of low railpad and high subgrade stiffness was shown preferable, in view of the long-term performance, for all operational regimes.

5. Acknowledgements

The study carried out in this paper is part of a long-term research program aiming at an improved understanding of the physics of track degradation and environmental vibration radiation under train loading. The program is executed by Delft University of Technology with financial support from the Dutch rail infra manager ProRail. The authors would like to thank especially Arjen Zoeteman from ProRail for his commitment to make scientific work in this domain possible.

References

[1] M. Sadri, M. Steenbergen, Effects of railway track design on the expected degradation: Parametric study on energy dissipation, Journal of Sound and Vibration, 419 (2018) 281-301.

[2] M.J. Brough, G. Ghataora, A.B. Stirling, K.B. Madelin, C.D. Rogers, D.N. Chapman, Investigation of railway track subgrade. Part 2: Case study, in: Proceedings of the Institution of Civil Engineers-Transport, Thomas Telford Ltd, 2006, pp. 83-92.

[3] Y. Sato, Japanese studies on deterioration of ballasted track, Veh. Syst. Dyn. 24 (suppl) (1995) 197-208.

[4] R. Fröhling, Deterioration of Railway Track Due to Dynamic Vehicle Loading and Spatially Varying Track Stiffness, Ph.D. thesis, University of Pretoria, Pretoria, South Africa, 1997.

[5] T. Dahlberg, Some railroad settlement models - a critical review, Proc. Inst. Mech. Eng. Part F J. Rail Rapid Transit 215 (F4) (2001) 289-300.

[6] T. R. Sussman, W. Ebersöhn, E. T. Selig, Fundamental nonlinear track load-deflection behavior for condition evaluation, Transportation Research Record 1742.1 (2001) 61-67.

[7] E. Berggren, Å. Jahlénius, B.-E. Bengtsson, Continuous track stiffness measurement: an effective method to investigate the structural conditions of the track, (2002).

[8] E.G. Berggren, Railway Track Stiffness. Dynamic Measurements and Evaluation for Efficient Maintenance, Ph.D. thesis, Royal Institute of Technology (KTH), 2009.

[9] L. Le Pen, D. Milne, D. Thompson, W. Powrie, Evaluating railway track support stiffness from trackside measurements in the absence of wheel load data. Canadian Geotechnical Journal, 53 (7) (2016), 1156-1166.
[10] P. Wang, L. Wang, R. Chen, J. Xu, J. Xu, M. Gao, Overview and outlook on railway track stiffness measurement. Journal of Modern Transportation, 24 (2) (2016), 89-102.
[11] A. Lundqvist, T. Dahlberg, Load impact on railway track due to unsupported sleepers, Proceedings of the Institution of Mechanical Engineers, Part F: Journal of Rail and Rapid Transit, 219 (2) (2005) 67-77.
[12] S. Zhang, X. Xiao, Z. Wen, X. Jin, Effect of unsupported sleepers on wheel/rail normal load, Soil Dynamics and Earthquake Engineering, 28 (8) (2008) 662-673.
[13] Y. Bezin, S.D. Iwnicki, M. Cavalletti, E. De Vries, F. Shahzad, G. Evans, An investigation of sleeper voids using a flexible track model integrated with railway multi-body dynamics, Proceedings of the Institution of Mechanical Engineers, Part F: Journal of Rail and Rapid Transit, 223 (6) (2009) 597-607.
[14] J.J. Zhu, A. Ahmed, S. Rakheja, A. Khajepour, Development of a vehicle–track model assembly and numerical method for simulation of wheel–rail dynamic interaction due to unsupported sleepers, Vehicle System Dynamics, 48 (12) (2010) 1535-1552.
[15] A. Recuero, J. Escalona, A. Shabana, Finite-element analysis of unsupported sleepers using three-dimensional wheel–rail contact formulation, Proceedings of the Institution of Mechanical Engineers, Part K: Journal of Multi-body Dynamics, 225 (2) (2011) 153-165.
[16] J. Zhu, D. Thompson, C. Jones, On the effect of unsupported sleepers on the dynamic behaviour of a railway track, Vehicle System Dynamics, 49 (9) (2011) 1389-1408.
[17] J. Shi, A.H. Chan, M.P. Burrow, Influence of unsupported sleepers on the dynamic response of a heavy haul railway embankment, Proceedings of the Institution of Mechanical Engineers, Part F: Journal of Rail and Rapid Transit, 227 (6) (2013) 657-667.
[18] A. Metrikine, A. Wolfert, H. Dieterman, Transition radiation in an elastically supported string. Abrupt and smooth variations of the support stiffness, Wave motion, 27 (4) (1998) 291-305.
[19] L. Andersen, S.R. Nielsen, Vibrations of a track caused by variation of the foundation stiffness, Probabilistic Engineering Mechanics, 18 (2) (2003) 171-184.
[20] S. Verichev, A. Metrikine, Instability of vibrations of a mass that moves uniformly along a beam on a periodically inhomogeneous foundation, Journal of Sound and Vibration, 260 (5) (2003) 901-925.
[21] Z. Dimitrovová, J. Varandas, Critical velocity of a load moving on a beam with a sudden change of foundation stiffness: Applications to high-speed trains, Computers & Structures, 87 (19-20) (2009) 1224-1232.

[22] Z. Dimitrovová, A general procedure for the dynamic analysis of finite and infinite beams on piece-wise homogeneous foundation under moving loads, Journal of Sound and Vibration, 329 (13) (2010) 2635-2653.
[23] L. Baeza, H. Ouyang, A railway track dynamics model based on modal substructuring and a cyclic boundary condition, Journal of Sound and Vibration, 330 (1) (2011) 75-86.
[24] K.K. Ang, J. Dai, Response analysis of high-speed rail system accounting for abrupt change of foundation stiffness, Journal of Sound and Vibration, 332 (12) (2013) 2954-2970.
[25] M. Steenbergen, H. de Graaf, On the effect of wheel flat wear on dynamic wheel-rail interaction force levels, in: The international conference on bogies, Budapest, Hungary, 2013, pp. 9-12.
[26] M.J.M.M. Steenbergen, Modelling of wheels and rail discontinuities in dynamic wheel–rail contact analysis, Vehicle System Dynamics, 44 (10) (2006) 763-787.